arXiv:1608.02747v1 [physics.optics] 9 Aug 2016

Near-field relaxation of a quantum emitter to 2D semiconductors: surface dissipation and exciton polaritons

Vasilios D. Karanikolas,* Cristian A. Marocico, Paul R. Eastham, and A. Louise Bradley
Photonics Group, School of Physics and CRANN,
Trinity College Dublin, College Green, Dublin 2, Ireland
(Dated: August 10, 2016)

The total spontaneous emission rate of a quantum emitter in the presence of an infinite MoS_2 monolayer is enhanced by several orders of magnitude, compared to its free-space value, due to the excitation of surface exciton polariton modes and lossy modes. The spectral and distance dependence of the spontaneous emission rate are analyzed and the lossy-surface-wave, surface exciton polariton mode and radiative contributions are identified. The transverse magnetic and transverse electric exciton polariton modes can be excited for different emission frequencies of the quantum emitter, and their contributions to the total spontaneous emission rate are different. To calculate these different decay rates, we use the non-Hermitian description of light-matter interactions, employing a Green's tensor formalism. The distance dependence follows different trends depending on the emission energy of quantum emitter. For the case of the lossy surface waves, the distance dependence follows a z^{-n}, $n = 2,3,4$, trend. When transverse magnetic exciton polariton modes are excited, they dominate and characterize the distance dependence of the spontaneous emission rate of a quantum emitter in the presence of the MoS_2 layers. The interaction between a quantum emitter and a MoS_2 superlattice is investigated and we observe a splitting of the modes supported by the superlattice. Moreover, a blue shift of the peak values of the spontaneous emission rate of a quantum emitter is observed as the number of layers is increased. The field distribution profiles, created by a quantum emitter, are used to explain this behavior.

PACS numbers: 33.80.-b, 42.50.-p, 73.20.Mf

I. INTRODUCTION

The emission properties of quantum emitters are modified by their environment [1]. In particular, through excitation of surface plasmon modes, the spontaneous emission rate of a quantum emitter (QE) can be enhanced by several orders of magnitude compared with its free-space value [2, 3]. Surface plasmon polaritons are collective oscillations of electrons and the electromagnetic field that are excited at the interface between a dielectric and a conductor, and they are confined at this interface and propagate along it. Noble metals, such as Au and Ag, are typically used as plasmonic materials. However, the main disadvantage of using noble metals is the fact that they have high losses in the optical region of the spectrum [4]. As an alternative for materials supporting surface plasmon modes, but with lower losses, graphene can be considered [5, 6]. Graphene is a zero direct band-gap two-dimensional material of great potential and with high mechanical capabilities [7]. However, it also has a disadvantage, since it exhibits no plasmonic response in the visible part of the spectrum, and acts only as a quencher when interacting with quantum emitters emitting in the visible part of the spectrum [8, 9].

In addition to surface plasmon modes, there are other surface modes such as phonon and exciton polariton [10, 11] modes. In previous years, a new family of two-dimensional materials, the transition metal dichalconides (TMD), such as MoS_2, SnS_2 and WeS_2, have been subject of intense theoretical [12–14] and experimental investigations [15, 16]. These materials are direct bandgap semiconductors, with the conduction and valence band edges at the doubly degenerate corners ($\pm\mathbf{K}$ points) of the hexagonal Brilouin zone, and can have relatively high absorption and intense photoluminescence [17, 18]. We calculate the spontaneous emission rate for a QE above a MoS_2 layer, and find that the spontaneous emission rate is enhanced by many orders of magnitude. We trace this effect to the near-field energy transfer from the QE to the surface exciton polariton. In addition to implications for energy transfer applications, such as photodetectors [19], photovoltaic [20] and light emitting devices [21–23], our results show that low-dimensional materials can be used to study polaritons and exciton-photon coupling phenomena without requiring a microcavity [24]. Herein we demonstrate that MoS_2 monolayers can support surface exciton polariton modes and their influence on the optical properties of QEs is substantial.

The interaction between quantum emitters (QEs) and multilayers of TMD materials is of particular experimental interest. Many applications can benefit from manipulating these interactions, such as photodetectors [19], electronic [25], photovoltaic [20] and light emitting devices [21–23]. Investigating the spectral and distance dependence of the interactions between QEs and TMD layers or monolayers is of absolute importance for such applications. Various experimental studies have been performed regarding the investigation of such interactions, and they report contradicting results concerning the power law followed by the interaction distance between the QE–TMD layers, where different QEs are considered for each case [26–31]. A systematic analysis is needed to account for the spectral and distance dependence of the QE–TMD layer interaction. Here we focus on material parameters describing the semiconducting behavior of MoS_2, through the exciton energies and damping parameters [17, 24, 32].

We find that transverse electric (TE) and transverse mag-

*Electronic address: karanikv@tcd.ie

netic (TM) exciton polariton modes are supported by a MoS_2 layer, Fig. 3. The propagation length and penetration depth of these modes are investigated. The SE rate of the QE is enhanced several orders of magnitude for emission energies close to the exciton energies, especially when the TM exciton polariton modes are excited, in the presence of a single MoS_2 layer, see Fig. 6. The different contributions to the total SE rate are presented: the lossy surface wave (LSW), TE and TM exciton polariton modes, and radiative emission contribution, for different QE–MoS_2 separations and emission energies of the QE.

Additional physics appears as one goes beyond the single layer structure to multilayers. In particular, we show that the electromagnetic coupling between the layers splits the degeneracy of the exciton polariton modes, even in the absence of direct electronic coupling. We find, Fig. 7, that the electromagnetic coupling between the layers leads to a blue-shift in the peak of the spontaneous emission rate with increasing number of layers. This may provide an explanation for the apparent different dependences of the emission rate with the layer number observed in experiments [29, 30].

In Sec. II we introduce the mathematical method for studying the QE–MoS_2 structure. The QE is described as a two-level system and the Green's tensor formalism is used to describe the light-matter interaction in the non-Hermitian description of quantum electrodynamics, II A. The optical response of the MoS_2 layer is modeled by the surface conductivity, Sec. II B. In Sec. III we give the results. We start in Sec. III A by analyzing the surface exciton polariton when a single exciton resonance is considered in the surface conductivity. When two exciton resonances are considered, we see that two bands are formed, corresponding to the TE and TM exciton polariton modes, Sec. III A. The propagation length and penetration depth of the TE and TM exciton polariton modes are analyzed. In Sec. III B, the interaction between a QE and a free-standing MoS_2 layer is considered. The spectral and distance dependence is analyzed and the different contributions are studied. The LSW, TE and TM exciton polariton modes and radiative emission contributions to the SE rate of a QE, at different positions and emission energies, are presented. In Sec. III C we focus on the interaction between a QE and MoS_2 planar superlattices. We observe that the TE and TM exciton polariton modes bands are still split and that multibands are also formed, due to interlayer scattering. The SE peak of the QE is blue-shifted and the absolute value of the SE rate enhancement decreases. Finally, in Sec. IV we give some concluding results and future steps for research in the field.

II. MATHEMATICAL METHODS

A. Spontaneous emission rate

The quantum emitters (QEs) considered in this paper are approximated as two-level systems. Various emitters, such as atoms, molecules, quantum dots and NV color centers, can be approximated in this way. The ground state of the QE is denoted as $|g\rangle$, and the excited state as $|e\rangle$. The transition frequencies from the excited to the ground state and the transition dipole matrix element are denoted as ω_T and μ, respectively. The multipolar Hamiltonian is used to describe a QE interacting with the electromagnetic field [33, 34], and it has the form

$$\hat{H} = \hat{H}_{\rm em} = \int d^3r \int_0^\infty d\omega\, \hbar\omega\, \hat{\mathbf{f}}^\dagger(\mathbf{r},\omega)\cdot\hat{\mathbf{f}}(\mathbf{r},\omega) + \hbar\omega_T \sigma^\dagger\sigma - \int d\omega \left[\hat{\mu}\cdot\hat{\mathbf{E}}(\mathbf{r},\omega) + H.c.\right], \tag{1}$$

where $\hat{\mu} = \mu\sigma^\dagger + \mu^*\sigma^-$ is the transition dipole operator of the two level system, with μ being the transition dipole moment of the system between its ground and excited states. The electric field operator has the form

$$\hat{\mathbf{E}}(\mathbf{r},\omega) = i\sqrt{\frac{\hbar}{\pi\varepsilon_0}}\frac{\omega^2}{c^2}\int d^3s\, \sqrt{\varepsilon''(\mathbf{s},\omega)}\,\mathfrak{G}(\mathbf{r},\mathbf{s},\omega)\cdot\hat{\mathbf{f}}(\mathbf{s},\omega), \tag{2}$$

where $\hat{\mathbf{f}}(\mathbf{s},\omega)$ and $\hat{\mathbf{f}}^\dagger(\mathbf{s},\omega)$ are creation and annihilation operators for medium-dressed states, which account for the various modes provided by the environment, such as the LSWs, surface exciton polariton and radiative modes considered in this paper.

An excited quantum emitter interacts with its environment through the electromagnetic field and relaxes from its excited state to the ground state by emitting a photon or exciting any of the dressed states supported by its environment. The initial state of the system is denoted as $|i\rangle = |e\rangle\otimes|0\rangle$, where the QE is in the excited state and the electromagnetic field is in its vacuum state. The quantum emitter will not stay indefinitely excited, but will relax to the medium dressed states and therefore the EM field will be in a $|1(\mathbf{k},p)\rangle = \hat{f}_i^\dagger(\mathbf{r},\omega)|0\rangle$ state; p and $\mathbf{k}$ are the polarization and wavevector, respectively. The final state of the entire system therefore has the form $|f\rangle = |g\rangle\otimes\hat{f}_i^\dagger(\mathbf{r},\omega)|0\rangle$. By applying Fermi's golden rule and summing over all final states, the expression for the SE rate Γ is obtained as:

$$\Gamma(\mathbf{r},\omega) = \frac{2\omega^2\mu^2}{\hbar\varepsilon_0 c^2}\hat{\mathbf{n}}\cdot\mathrm{Im}\,\mathfrak{G}(\mathbf{r},\mathbf{r},\omega)\cdot\hat{\mathbf{n}}, \tag{3}$$

where $\hat{\mathbf{n}}$ is a unit vector along the direction of the transition dipole moment, μ, and $\mathfrak{G}(\mathbf{r},\mathbf{s},\omega)$ is the Green's tensor representing the response of the geometry under consideration to a point-like excitation. In order to quantify the influence of the environment on the QE emission, the normalized SE rate is defined as:

$$\tilde{\Gamma} = \frac{\Gamma}{\Gamma_0} = \sqrt{\varepsilon} + \frac{6\pi c}{\omega}\hat{n}_i\mathrm{Im}\,\mathfrak{G}_{\rm S}^{ii}(\mathbf{r},\mathbf{r},\omega)\hat{n}_i, \tag{4}$$

where ε is the permittivity of the host medium, Γ_0 is given by the Einstein A-coefficient $\Gamma_0 = \omega^3\mu^2/3\pi c^3\hbar\varepsilon_0$ and $\mathfrak{G}_{\rm S}$ is the scattering part of the Green's tensor calculated at the QE position $\mathbf{r}$.

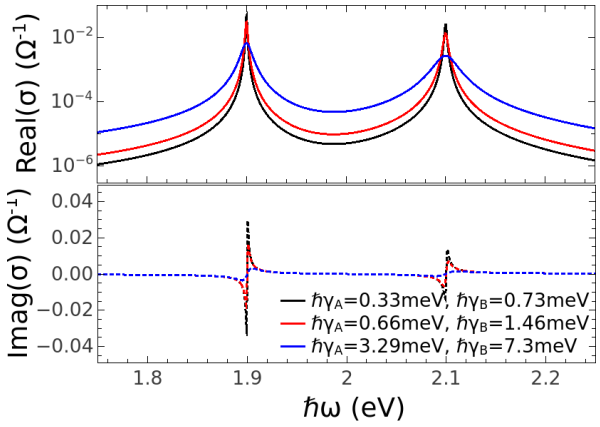

Figure 1: (Color online) Real and imaginary parts of the surface conductivity of MoS_2, $\sigma_{\rm res}$, given by Eq. (7) for different values of the damping parameters, $\hbar\gamma_A = 0.3\,$meV, $0.7\,$meV and $3.3\,$meV and $\hbar\gamma_B = 0.7\,$meV, $1.4\,$meV and $7.3\,$meV.

The normalized SE rate for the x and z orientations of the transition dipole moment of a QE in the presence of an infinite MoS_2 layer are given by the expressions

$$\tilde{\Gamma}_z = \sqrt{\varepsilon_1} + \frac{3c}{2\omega}\mathrm{Im}\left(i\int_0^\infty \mathrm{d}k_s \frac{k_s^3}{k_{z1}k_1^2} R_N^{11} e^{2ik_{z1}z}\right), \tag{5a}$$

$$\tilde{\Gamma}_x = \sqrt{\varepsilon_1} + \frac{3c}{4\omega}\mathrm{Im}\left[i\int_0^\infty \mathrm{d}k_s \frac{k_s}{k_1}\left(R_M^{11} + \frac{k_{z1}^2}{k_1^2} R_N^{11}\right) e^{2ik_{z1}z}\right]. \tag{5b}$$

More details on the calculation of the Green's tensor, when an infinite MoS_2 layer and superlattice are considered as the environment of a QE, are given in App. A.

Here R_N and R_M are Fresnel coefficients for the reflection from the surface, defined in Appendix A. For a single free-standing layer ($\varepsilon_1 = \varepsilon_2 = 1$), with surface conductivity σ they are [35, 36]

$$R_M^{11} = \frac{-\alpha k_0}{k_z + \alpha k_0}, \quad R_N^{11} = \frac{\alpha k_z}{k_0 + \alpha k_z} \tag{6a}$$

$$R_M^{21} = \frac{k_z}{k_z + \alpha k_0}, \quad R_N^{21} = \frac{k_0}{k_0 + \alpha k_z}, \tag{6b}$$

where $\alpha = 2\pi\sigma/c$ and $k_z = \sqrt{k_0^2 - k_s^2}$.

B. Surface conductivity

MoS_2 is a direct gap semiconductor with relatively intense photoluminescence [22]. The resonance part of the 2-dimensional optical conductivity of the MoS_2, $\sigma_{\rm res}$, takes into account the interaction of light with the lowest energy A and B excitons and is given by

$$\sigma_{\rm res}(\omega) = \frac{4\alpha_0\hbar c v^2}{\pi a_{\rm ex}^2 \omega}\sum_{k=A,B}\frac{-i}{E_k - \hbar\omega - i\hbar\gamma_k}, \tag{7}$$

where α_0 is the fine structure constant, $a_{\rm ex} = 0.8\,$nm is the exciton Bohr radius, the damping parameters are γ_A and γ_B, and the exciton energies are $E_A = 1.9\,$eV and $E_B = 2.1\,$eV. v is a constant velocity, which is connected with the hopping parameter, and for MoS_2 we use the value $v = 0.55\,$nm/fs [17, 32]. In Fig. 1 we present the real and imaginary parts of the surface conductivity for different values of the damping parameters, γ_A and γ_B[24]. The damping parameters, $\gamma_{\rm A}$ and $\gamma_{\rm B}$, are connected with the quality of the MoS_2 layer at different temperatures, and for that reason we choose to investigate a broader spectrum of parameters to account for the different mechanism of losses [37]. The real part of the surface conductivity, $\sigma_{\rm res}(\omega)$, is connected with the losses, the higher its values, the more lossy the material. We observe in Fig. 1 that as the value of the damping parameters increases, the peaks of the real part of the surface conductivity in Fig. 1 become broader. At the exciton energies, E_A and E_B, the losses are largest for the smallest value of the damping parameters, γ_A and γ_B, because they give the linewidth of the resonance, but away from them the real part of $\sigma_{\rm res}$ increases as the damping increases. The sign of the imaginary part of the surface conductivity, $\sigma_{\rm res}(\omega)$, determines the type of modes supported by the MoS_2 layer and how dispersive they are. More details on this will be given in the next section.

At even higher energies, the interband transitions need to be included in the model describing the surface conductivity. We model these transitions with an expression of the form

$$\mathrm{Real}\left(\sigma_{\rm inter}\right) = \frac{m\sigma_0\theta(\omega-\omega_B)}{\sqrt{1+2E_B\beta+\Omega^2}}\left[1 + \frac{1+2E_B\beta}{\Omega^2}\left(1 + E_B\beta - \sqrt{1+2E_B\beta+\Omega^2}\right)\right], \tag{8}$$

where $\hbar\omega_B = E_B$, $\Omega = \hbar\omega/E_B$ and β is a mixing parameter, for MoS_2 $E_B\beta = 0.84$ [38]. The parameter m is for scaling the absorption described by Eq. (8). As we will see in Sec. III A, the excitonic effects described by Eq. (8) are not important in

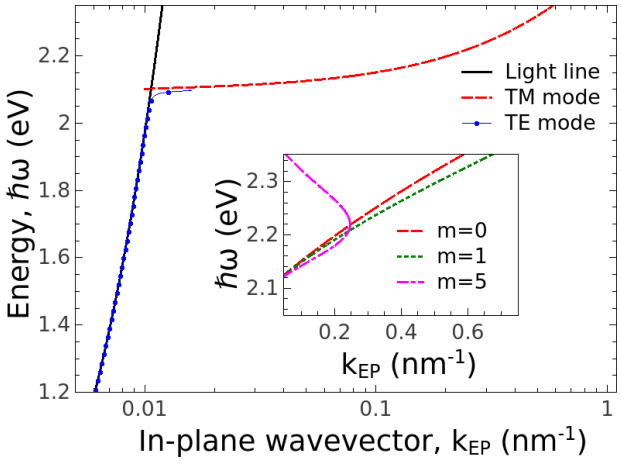

Figure 2: (Color online) Dispersion relation, $\mathrm{Re}(k_{\mathrm{EP}}(\omega))$, for a 2D free-standing material, when a single exciton is considered, $E_B = 2.1\,\mathrm{eV}$. The value of the damping parameter is $\gamma_B = 0.7\,\mathrm{meV}$. In the inset the dispersion relation is presented when the interband transitions are considered, Eq. 8a.

the energy spectrum we focus our analysis on, in particular for energies close to the exciton resonances E_A and E_B, $1.7\,\mathrm{eV} < \hbar\omega < 2.2\,\mathrm{eV}$.

The emphasis of this paper is to theoretically investigate light-matter interactions, thus, we choose to use a theoretical expression to describe the optical response of the MoS_2. This is done in order to keep the discussion as general as possible. We choose the material parameters connected with MoS_2, and these can be easily modified to study the interaction between a QE and any TMD superlattice or thin semiconducting quantum well. Furthermore, the material parameters for the MoS_2 are connected with the quality of a specific sample, and thus experimentally, they vary from study to study.

III. RESULTS

A. Surface exciton polariton modes

We start our analysis by considering a single exciton polariton mode shown in Fig. 2, supported by a two-dimensional material. The exciton energy is $E_B = 2.1\,\mathrm{eV}$ and the damping parameter has a value of $\hbar\gamma_B = 0.7\,\mathrm{meV}$. We use exactly the same parameters as when describing the MoS_2 layer, only ignoring the exciton with energy E_A. In Fig. 2 the band structure of the transverse electric (TE) and transverse magnetic (TM) exciton polariton modes for a free standing ($\varepsilon_1 = \varepsilon_2 = 1$) single exciton layer are shown. The dispersion relation of the TE exciton polariton mode is calculated by setting the denominator of R_M^{11}, Eq. (6a), to zero which gives

$$k_{\mathrm{EP}}^{\mathrm{TE}} = \frac{\omega}{c}\sqrt{1 - 4\pi^2\sigma_{\mathrm{res}}^2/c^2}. \tag{9}$$

The TE mode is supported by the MoS_2 layer only when the $\mathrm{Im}(\sigma_{\mathrm{res}}) < 0$, whereas for $\mathrm{Im}(\sigma_{\mathrm{res}}) > 0$ the TE mode is on the improper Riemann sheet [39]. $k_{\mathrm{EP}}^{\mathrm{TE}}$ is the in-plane wave vector of the TE exciton polariton mode propagating on the MoS_2 layer. The available TM modes are found similarly by setting the denominator of the reflection coefficient R_N^{11}, Eq. (6a), to zero and we get the expression

$$k_{\mathrm{EP}}^{\mathrm{TM}} = \frac{\omega}{c}\sqrt{1 - c^2/4\pi^2\sigma_{\mathrm{res}}^2}, \tag{10}$$

which gives the dispersion relation $k_{\mathrm{EP}}^{\mathrm{TM}}(\omega)$, the relation between the frequency, ω, and the TM exciton polariton mode in-plane wave vector, $k_{\mathrm{EP}}^{\mathrm{TM}}$. The TM exciton polariton modes can propagate on the MoS_2 layer only when $\mathrm{Im}(\sigma_{\mathrm{res}}) > 0$, whereas when $\mathrm{Im}(\sigma_{\mathrm{res}}) < 0$ the TM mode given by Eq. (10) is on the improper Riemann sheet [40, 41].

For the case of a single exciton, the imaginary part of the surface conductivity is negative for energies below the exciton energy, $\hbar\omega < 2.1\,\mathrm{eV}$, thus allowing only TE exciton polariton modes to propagate. On the other hand for $\hbar\omega > 2.1\,\mathrm{eV}$, above the exciton energy E_B, only TM exciton polariton modes are supported. As we observe in Fig. 2, the TE modes are very close to the light-line, which means that these modes are loosely confined to the MoS_2 layer. It is only very close to the exciton energy, E_B, that they start to become dispersive. The TM modes are clearly more dispersive and they are tightly confined to the MoS_2 layer.

In the inset of Fig. 2 the TM exciton polariton mode is presented for energies $\hbar\omega > E_B$, in the case when interband transitions are also included, Eq. (8). We consider the case of $m = 0$, 1 and 5 in Eq. (8). We observe that as the value of m is increased, the dispersion relation, $\mathrm{Re}\left(k_{\mathrm{EP}}^{\mathrm{TM}}(\omega)\right)$, starts to bend back, towards the light line, for high energies, $\hbar\omega \gtrsim 2.2\,\mathrm{eV}$. This is due to the higher losses caused by electron-hole pair generation. The dispersion relation has similar behavior to noble metal thin films at higher energies [42]. We observe that at energies up to $2.2\,\mathrm{eV}$, the dispersion lines, for the different values of m, are very close. For that reason, in the rest of this paper we ignore the effect of the interband transitions, which are small in the energy range we investigate, $1.7\,\mathrm{eV} < \hbar\omega < 2.2\,\mathrm{eV}$.

We turn the discussion now to the case in which we consider both excitons in the surface conductivity, σ_{res}, which matches the physical material parameters of MoS_2, Eq. (7). In Fig. 3a we present a plot of the dispersion relation, $\mathrm{Re}\,(k_{\mathrm{EP}}(\omega))$, for the TE and TM exciton polariton modes. Due to the presence of two excitons with energies $E_A = 1.9\,\mathrm{eV}$ and $E_B = 2.1\,\mathrm{eV}$, the TE and TM exciton polariton modes split into two branches [43]. Again, an analogy can be drawn with the case of a metallic thin film, which is sandwiched between two materials with different dielectric permittivities [42]. Two surface plasmon polariton modes are present in this case, due to the two different metal-dielectric interfaces. In our case, the presence of the two excitons, with close energies, is the reason for the dispersion relation in Fig. 3. It implies that there is a change of sign for $\mathrm{Im}\,(\sigma_{\mathrm{res}})$, Fig. 1. In particular, for energies $\hbar\omega < E_A$ the imaginary part of the surface conductivity is negative $\mathrm{Im}\,(\sigma_{\mathrm{res}}) < 0$, thus only TE exciton polariton modes are supported, Fig. 3a. These modes lie very close to the light line and are only loosely confined to the

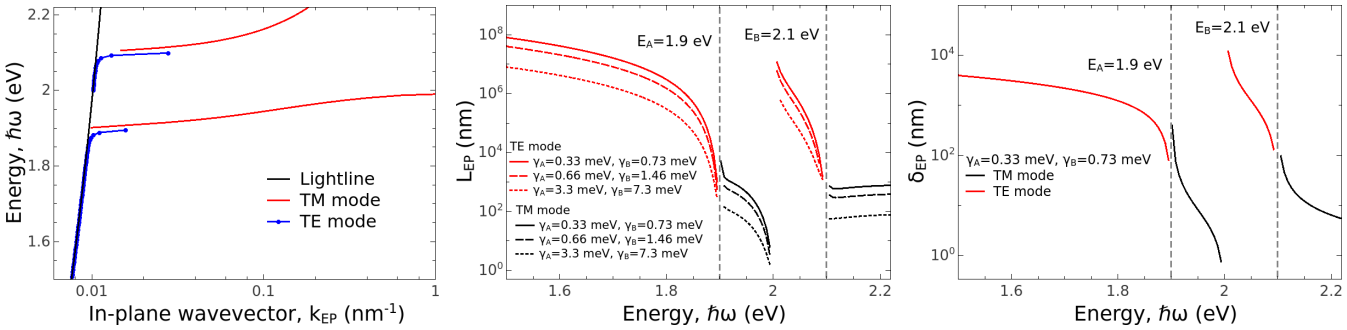

Figure 3: (Color online) (a) Plot of the dispersion relation, $\mathrm{Re}(k_{\mathrm{EP}}(\omega))$, when a free standing MoS_2 monolayer, $\varepsilon_1 = \varepsilon_2 = 1$, is considered. (b-c) Plot of the propagation length, L_{EP}, and the penetration depth, δ_{EP}, respectively. Different values of the damping parameters, γ_A and γ_B, are considered. More details in the legends.

MoS_2 layer and only very close to the exciton energy E_A do they become more dispersive. At energies $E_A < \hbar\omega < 2\,\mathrm{eV}$ the $\mathrm{Im}(\sigma_{\mathrm{res}}) > 0$, thus TM exciton polariton modes are supported which are highly dispersive and the value of the in-plane wave vector, $k_{\mathrm{EP}}^{\mathrm{TM}}$, is larger by up to two orders of magnitude than the free-space wavevector, $k_0 = \omega/c$. At the energy of $\hbar\omega = 2\,\mathrm{eV}$, $\mathrm{Im}(\sigma_{\mathrm{res}}) \approx 0$ and at this point the imaginary part of the surface conductivity now changes sign from plus to minus, due to the interaction between the two exciton resonances; thus, for energies $2\,\mathrm{eV} < \hbar\omega < E_B$, we have $\mathrm{Im}(\sigma_{\mathrm{res}}) < 0$, and TE exciton polariton modes are supported. For $\hbar\omega > E_B$, $\mathrm{Im}(\sigma_{\mathrm{res}}) > 0$ and TM exciton polariton modes are again supported. In Fig. 3a we consider as damping parameters the values $\hbar\gamma_A = 0.33\,\mathrm{meV}$ and $\hbar\gamma_B = 0.70\,\mathrm{meV}$, and increasing these values shows small influence on the real part of the in-plane wavevector of the exciton polariton mode, k_{EP}. $\lambda_{\mathrm{EP}} = 2\pi/k_{\mathrm{EP}}$ gives the propagation wavelength of the exciton polariton mode.

The imaginary part of the in-plane wavevector, k_{EP}, is connected with the propagation length of the exciton polariton mode $L_{\mathrm{EP}} = 1/\mathrm{Im}(k_{\mathrm{EP}})$. In Fig. 3b the propagation length, L_{EP}, is shown as a function of energy for different values of the damping parameters, γ_A and γ_B (see the legend of Fig. 3b for more details). We again observe the different intervals where the TE or TM exciton polariton modes are excited, depending on the sign of $\mathrm{Im}(\sigma_{\mathrm{res}})$. As we have already pointed out, the TE modes are loosely confined to the MoS_2 layer, thus their propagation length is very large and its value differs from the TM exciton polariton modes propagation length by up to 6 orders of magnitude. As the damping is increased, the propagation length, L_{EP}, decreases. It is also seen that the real part of the surface conductivity, σ_{res}, which is connected with the material losses, increases at energies of the exciton resonances with increasing damping, Fig. 1.

The penetration depth is defined as $\delta_{\mathrm{EP}} = 1/\mathrm{Im}\left(k_z^{\mathrm{EP}}\right)$, where $k_z^{\mathrm{EP}} = \sqrt{k_0^2 - k_{\mathrm{EP}}^2}$, and is connected with the extent of the exciton polariton mode in the direction perpendicular to the MoS_2 layer. In Fig. 3c the penetration depth is presented as a function of energy with damping parameters $\hbar\gamma_A = 0.33\,\mathrm{meV}$ and $\hbar\gamma_B = 0.70\,\mathrm{meV}$. Again, the sign of $\mathrm{Im}(\sigma_{\mathrm{res}})$ gives the different intervals where the TE and TM exciton polariton modes propagate. The TE modes are only loosely confined to the MoS_2 layer, are essentially radiative modes, as we will see in the next section, and have only a small contribution to the modification of the emission properties of a QE in proximity to the MoS_2 layer.

B. Spontaneous emission in the presence of a single MoS_2 layer

In this section we will investigate the interaction between a QE and a MoS_2 layer. In Fig. 4 we investigate the spontaneous emission rate when we consider a QE at a fixed position above a free-standing MoS_2 layer, as a function of its emission energy, and both x- and z- orientations for the transition dipole moment of the QE are considered, (4a-4b) and (4c-4d) respectively. The total spontaneous emission is analyzed over the lossy-surface-wave, exciton polariton mode and radiative emission contributions. The damping parameters have the values $\hbar\gamma_A = 0.33\,\mathrm{meV}$ and $\hbar\gamma_B = 0.70\,\mathrm{meV}$.

In Fig. 4a the QE is positioned at $\mathbf{r}_{\mathrm{QE}} = (0, 0, 2\,\mathrm{nm})$. Due to the orientation of the transition dipole moment along x, TE and TM exciton polariton modes are supported by a MoS_2 layer, depending on the sign of the $\mathrm{Im}(\sigma_{\mathrm{res}})$, as we have already discussed in Sec. II B. The contributions of these modes are obtained by extracting the pole contributions from Eq. (5b), which for $\varepsilon_1 = \varepsilon_2 = 1$, have the form:

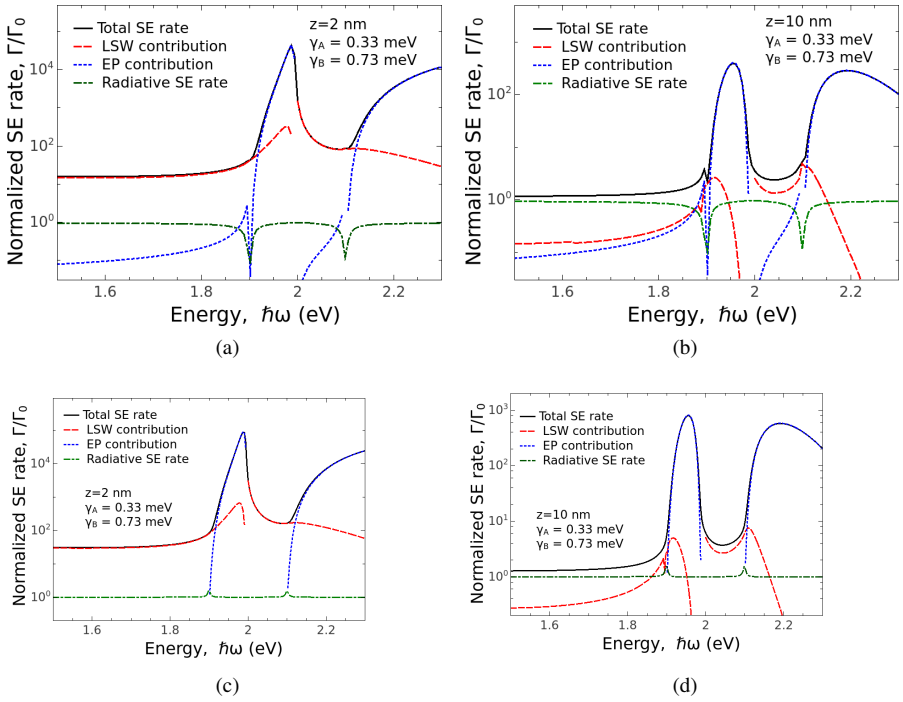

Figure 4: (Color online) The total normalized spontaneous emission of a QE, $\tilde{\Gamma}$, placed at a fixed position as a function of its emission energy, is analyzed with respect to the lossy-surface-wave, surface-mode and radiative emission contributions. The transition dipole moment of the QE is oriented along x (a-b) and z (c-d). (a,c) $\mathbf{r}_{\rm QE} = (0,0,2\,{\rm nm})$. (b,d) $\mathbf{r}_{\rm QE} = (0,0,10\,{\rm nm})$. The values of the damping parameters considered are $\gamma_A = 0.3\,{\rm meV}$ and $\gamma_B = 0.7\,{\rm meV}$.

$$\tilde{\Gamma}_{x,\rm EP}(\omega,\mathbf{r}_{\rm QE}) = \frac{3\pi c}{4\omega}{\rm Im}\left[\frac{\alpha^2 k_0^2}{k_{z1}^{\rm TE}}\,{\rm e}^{2ik_{z1}^{\rm TE}z_{\rm QE}}\Theta\left(-{\rm Im}\left(\sigma_{\rm res}\right)\right) - \frac{k_{z1}^{\rm TM}}{\alpha^2}\,{\rm e}^{2ik_{z1}^{\rm TM}z_{\rm QE}}\Theta\left({\rm Im}\left(\sigma_{\rm res}\right)\right)\right] \tag{11}$$

where $k_{z1}^i = \sqrt{k_0^2 - \left(k_{\rm EP}^i\right)^2}$, for $i = {\rm TE,TM}$ and where $k_{\rm EP}^i$ are given by Eqs. (9) and (10), respectively. The LSWs contribution is obtained in the large k_s limit of the integrand of Eq. (5b) [44]and has the form

$$\tilde{\Gamma}_{x,\rm LSW}(\omega,\mathbf{r}_{\rm QE}) = \frac{3c}{4\omega}{\rm Im}\left[\int_K^\infty {\rm d}k_s\left(\frac{-\alpha k_0}{ik_s+\alpha k_0} + \frac{1}{k_0^2}\frac{i\alpha k_s^3}{k_0+i\alpha k_s}\right){\rm e}^{-2k_s z_{\rm QE}}\right], \tag{12}$$

where the lower limit on the integral is used for numerical reasons to separate the various contributions to the full integral. In particular, when there are no TM exciton polariton modes and the TE exciton polariton modes lie very close to the light line, $K \simeq k_0$. When the TM modes are present, the lower integration limit should be $K > {\rm Re}\left(k_{\rm EP}^{\rm TM}\right)$, in order not to include the pole contribution, given by Eq. (11). The LSWs are non-propagating dissipative modes. The radiative contribution is given by integrating Eq. (5b) over the interval $[0,k_0]$.

In Fig. 4a, for emission energies of the QE below the first exciton energy, $\hbar\omega < E_A$, the QE's near-field can excite LSWs and these lossy modes are the main contribution to the total SE rate of the QE. Exciting the TE exciton polariton mode makes a small contribution to the total SE rate. As the emission energy of the QE is increased, in the interval $E_A < \hbar\omega < 2\,{\rm eV}$, the TM exciton polariton mode contribution dominates as the main channel of relaxation for the total SE rate, although the LSW still have a considerable contribution. At emission energies in the interval $2\,{\rm eV} < \hbar\omega < E_B$, the LSW again dominate and the contribution of the TE exciton polariton modes is small. As we have already argued, the TE exciton polariton modes are loosely confined to the MoS_2 layer, and thus their contribution to the normalized SE rate is small, see Eq. (11). Finally, for emission energies $\hbar\omega > E_B$, the TM exciton polariton mode contribution dominates and the LSW is

suppressed, although its contribution is still considerable.

In Fig. 4b we observe that the enhancement of the total normalized SE rate of the QE placed at $\mathbf{r}_{\rm QE} = (0,0,10\,{\rm nm})$, is smaller when compared with the case presented in Fig. 4a. This is due to the fact that the near-field of the QE decouples from the MoS_2 layer as the QE–MoS_2 layer distance is increased. Thus, the LSW contribution to the total SE rate along the whole spectrum is small. The LSWs can only be excited at small QE–MoS_2 separations. The TE modes also have a small contribution to the total SE rate, but they can now compete with the LSWs. However, the TM exciton polariton modes, in the interval where they are excited, dominate the total SE rate of the QE. The SE rate is enhanced several orders of magnitude in those intervals, compared with the free-space value.

When the transition dipole moment of the QE is along z, the pole contribution to Eq. (5a) comes exclusively from the TM exciton polariton mode and has the form:

$$\tilde{\Gamma}_{z,{\rm EP}}(\omega,\mathbf{r}_{\rm QE}) = -\frac{3\pi c^2}{2\omega^2}{\rm Im}\left[\frac{\left(k_{\rm EP}^{\rm TM}\right)^2}{\alpha}{\rm e}^{2ik_{z1}^{\rm TM}z_{\rm QE}}\right], \qquad (13)$$

where $k_{z1}^{\rm TM} = \sqrt{k_0^2 - \left(k_{\rm EP}^{\rm TM}\right)^2}$. The LSW contribution, obtained in the limit $k_s \to \infty$ of Eq. (5a), has the form

$$\tilde{\Gamma}_{z,{\rm LSW}}(\omega,\mathbf{r}_{\rm QE}) = \frac{3c}{2\omega k_0^2}{\rm Im}\left[\int_K^\infty {\rm d}k_s \frac{i\alpha k_s^3}{k_0 + i\alpha k_s}{\rm e}^{-2k_s z_{\rm QE}}\right], \qquad (14)$$

where the lower limit is determined by the existence of a TM exciton polariton mode, $K > k_{\rm EP}^{\rm TM}$ when present, and by $K \geqslant k_0$ when absent. The radiative contribution, $\tilde{\Gamma}_{z,0}(\omega,\mathbf{r}_{\rm QE})$, is given by integrating Eq. (5a) over the interval $[0,k_0]$.

In Fig. 4c we investigate the case for which the transition dipole moment of the QE is along z, at $\mathbf{r}_{\rm QE} = (0,0,2\,{\rm nm})$, showing the SE rate as a function of the QE emission energy. Due to the dipole orientation, only TM exciton polariton modes are excited in the intervals $E_A < \hbar\omega < 2\,{\rm eV}$ and $\hbar\omega > E_B$ and these are the main channels of relaxation of the QE. The LSWs dominate the total SE rate outside the interval where TM exciton polariton modes are excited, although they also make a considerable contribution in the range $E_A < \hbar\omega < 2\,{\rm eV}$. In Fig. 4d the distance between the QE and the MoS_2 layer is increased to $\mathbf{r}_{\rm QE} = (0,0,10\,{\rm nm})$. The LSWs contribution decreases as the distance between QE and the MoS_2 layer increases. The total SE rate is enhanced several orders of magnitude when the TM exciton polariton mode is excited. In general, the SE rate of a QE has similar characteristics for the x and z polarizations. The main difference is that, for a QE with a transition dipole moment along x, TE exciton polariton modes can be excited. The coupling between a QE and the MoS_2 layer is more efficient for the z orientation. For the rest of this paper we focus on a QE with z orientation of the transition dipole moment.

The distance dependence of the interaction between QEs and a TMD monolayer has been investigated experimentally and different theoretical expressions have been used to fit the experimental results. In ref. [31] they report a z^{-4} behavior of the distance dependence of the interaction between a QE and a $MoSe_2$ layer, although the authors fit the intensity quenching rather than the lifetime quenching. On the other hand, ref. [28] uses multiple QEs and investigates their lifetime quenching in the presence of a MoS_2 monolayer. The extracted fittings for the lifetime quenching are between z^{-3} to z^{-4}.

In Fig. 5 we present the distance dependence of the spontaneous emission rate of a QE, placed at $\mathbf{r}_{\rm QE} = (0,0,z_{\rm QE})$, and oriented along z, for fixed emission energies. We analyze the different contributions to the total SE rate, the LSWs, TM exciton polariton modes and the radiative emission using Eqs. (5a), (13) and (14). We consider four values of the emission energy of the QE, one in the range $\hbar\omega < E_A$, where the LSWs dominate and one in the $E_A < \hbar\omega < 2\,{\rm eV}$ range, where the TM exciton polariton modes are excited. The other two values are at $\hbar\omega = 1.9\,{\rm eV}$, right on the exciton energy E_A, and $\hbar\omega = 2.0\,{\rm eV}$, at the position where ${\rm Im}(\sigma_{\rm res})$ changes sign due to the interaction between the two excitons.

In Fig. 5a the QE emission energy is $\hbar\omega = 1.5\,{\rm eV}$, in the interval $\hbar\omega < E_A$, thus we see that the main contribution comes from the LSWs very close to the MoS_2 layer, but this channel of interaction dies out quickly and, at separations as small as $z_{\rm QE} \approx 8\,{\rm nm}$, the SE rate reverts to its free-space value. At this energy there is no exciton polariton mode, due to the dipole moment orientation of the QE. The integral in Eq. (14) has contributions of the form $A_1/z^2 + A_2/z^3 + A_3/z^4$, therefore in order to analyze the LSW contribution, we use the fitting expression:

$$f(z) = A\,z^n \qquad (15)$$

and in Fig. 5a we show that $n = -2.5$. This fitting shows that the behavior of MoS_2 layer is very different to the case of a graphene layer in the optical part of the spectrum. The optical response of graphene, in the optical part of the spectrum, is constant and characterized by a surface conductivity of $\sigma_{\rm Graph} = \sigma_0 = e^2/2\hbar$. The distance dependence of the SE rate of a QE is then given by $\tilde{\Gamma} \propto 1/z^4$, Eq. (14), which is a universal scaling law of the distance dependence between a QE and a graphene monolayer, in the optical part of the spectrum [8, 9, 30]. In Fig. 5b the QE energy is $\hbar\omega = E_A = 1.9\,{\rm eV}$, and we observe a behavior similar to Fig. 5a, but now the fitting of the LSWs, which have the largest contribution to the total SE rate, gives $n \approx -2$ and the QE reverts to the radiative value of the SE at distances of 10 nm. We furthermore observe that the radiative SE rate of the QE is enhanced very close to the MoS_2, which is an effect of constructive interference with the image dipole, due to the dipole orientation.

In Fig. 5c the emission energy of the QE is $\hbar\omega = 1.915\,{\rm eV}$ and we observe that the main contribution to the SE rate close to the MoS_2 layer again comes from the LSWs. At this energy a TM exciton polariton mode is excited and thus adds a new path of relaxation for the QE. The TM exciton polariton mode has a considerable contribution at small separations between the QE and the MoS_2 layer and dominates at intermediate distances, $6\,{\rm nm} < z_{\rm QE} < 100\,{\rm nm}$. In order to better understand the influence of the TM modes on the SE rate, we use a fitting expression of the form:

$$g(z_{\rm QE}) = A\,\exp(-2z_{\rm QE}/B), \qquad (16)$$

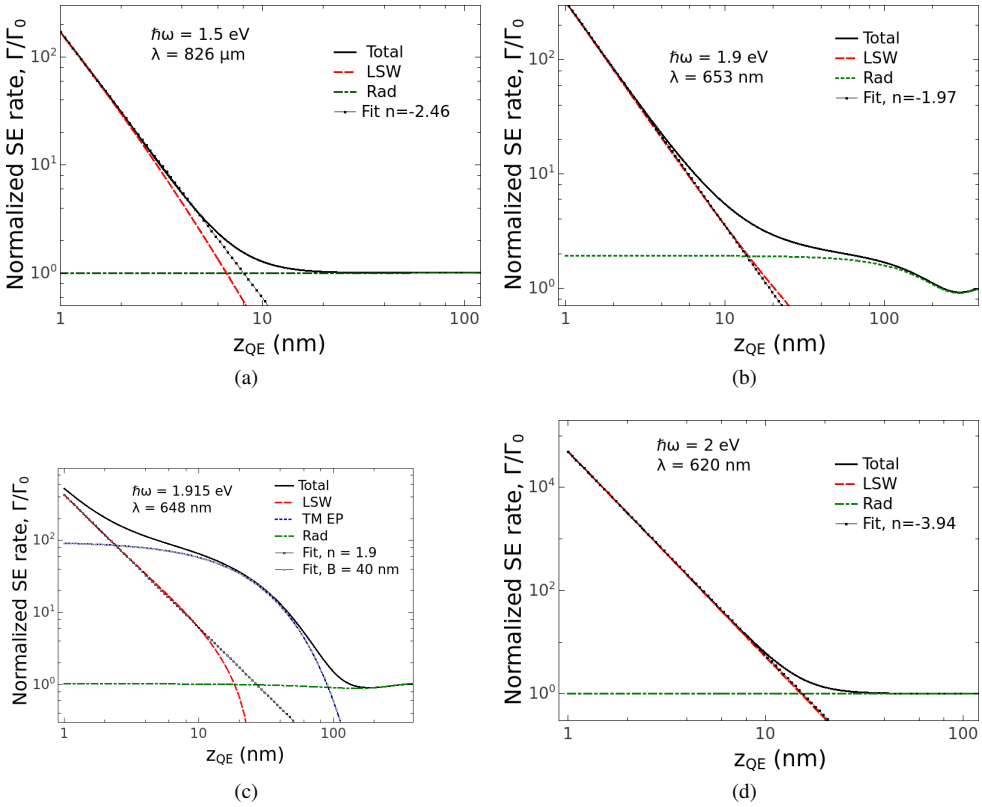

Figure 5: (Color online) The total normalized spontaneous emission rate of a QE, with fixed emission energy as a function of its position $\mathbf{r} = (0,0,z_{\rm QE})$, is analyzed with respect to the lossy-surface-wave, exciton polariton mode and radiative emission contributions. The transition dipole moment of the QE is z-oriented. (a) $\hbar\omega = 1.5\,$eV. (b) $\hbar\omega = 1.9\,$eV. (c) $\hbar\omega = 1.915\,$eV (d) $\hbar\omega = 2.0\,$eV. The damping parameters have the values, $\gamma_B = 0.3\,$meV and $\gamma_A = 0.7\,$meV.

where B is the fitting parameter of interest, connected with the penetration depth of the TM exciton polariton mode, $\delta_{\rm EP} = 1/{\rm Im}\left(k_z^{\rm EP}\right)$. The value of the fitting parameter in Fig. 5c is found to be $B = 40\,$nm which is the same as the value plotted in Fig. 3c where $\delta_{\rm TM} = 40\,$nm. The distance dependence of LSWs is described by Eq. (15) with $n \approx -2$. The LSW contribution to the SE rate is calculated using the approximate expression Eq. (14). When the TM modes are also present, it becomes more challenging to distinguish between the propagating, TM exciton polariton, and non-propagating, LSW, nature of the relaxation. In Fig. 5d the emission energy is $\hbar\omega = 2\,$eV, and at this energy there is a change of sign of the ${\rm Im}(\sigma_{\rm MoS_2})$ from positive to negative values while the ratio ${\rm Re}\,(\sigma_{\rm res}))/{\rm Im}\,(\sigma_{\rm res}) \gg 1$, thus we can safely ignore the imaginary part. We then have a situation identical to graphene and the LSWs, which dominate at small QE–MoS_2 layer separations, follow a behavior given by Eq. (15) with $n \approx -4$.

For completeness we present the full spectral and distance dependence of the SE rate of a QE in the presence of a MoS_2 layer, in Fig. 6. This is a contour plot of the normalized total SE rate of a QE, as a function of the QE position, $\mathbf{r}_{\rm QE} = (0,0,z_{\rm QE})$, and its emission energy, $\hbar\omega$. The transition dipole moment of the QE is along z. The olive green line represents the boundary of the parameter space where $\Gamma/\Gamma_0 > 10$.

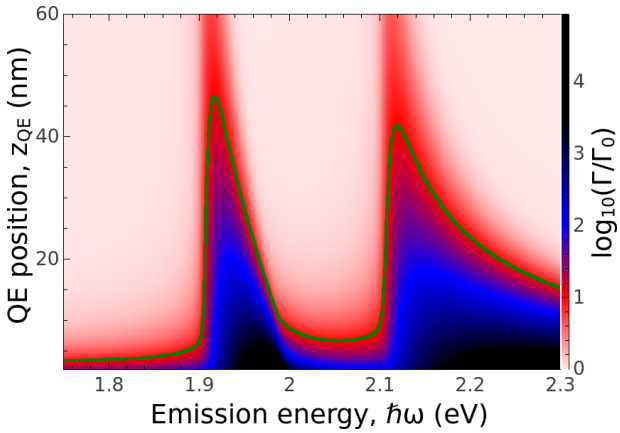

Figure 6: (Color online) Contour plot of the total normalized SE of a QE, as a function of its position, $\mathbf{r}_{\rm QE} = (0,0,z_{\rm QE})$, and emission energy, $\hbar\omega$. The transition dipole moment of the QE is z-oriented. The value of the damping parameters that are considered are $\gamma_A = 0.3\,$meV and $\gamma_B = 0.7\,$meV.

We observe that at emission energies where one can excite the TM exciton polariton mode supported by the MoS_2 layer, at $1.9\,{\rm eV} < \hbar\omega < 2\,{\rm eV}$ and $\hbar\omega > 2.1\,$eV, the SE rate is enhanced

up to 10 times, compared with its free-space value, for distances up to 40 nm. At small distances, the SE rate is enhanced due to the excitation of the non-propagating LSWs. The values of the damping parameters considered are $\hbar\gamma_A = 0.3\,\text{meV}$ and $\hbar\gamma_B = 0.7\,\text{meV}$.

C. Spontaneous emission in the presence of a superlattice of MoS_2 layers

In this section we investigate the influence of the presence of a superlattice composed of multiple MoS_2 layers on the emission properties of a QE. There are contradicting experimental reports regarding the influence on the SE rate of a QE interacting with TMD layers, as the number of layers is increased. In particular, in refs. [26, 30], the authors report that, as the number of MoS_2 layers is increased, the SE rate of the QEs decreases. The authors of ref. [30] use a bulk dielectric permittivity to describe the optical response of the MoS_2 and they attribute the decreasing behavior to dielectric screening [45]. In particular, they found that, by increasing the thickness of the MoS_2 slab, the field intensity created by a dipole source on the slab drops. The screening effect is connected with the difference between the parallel and perpendicular dielectric permittivities of the MoS_2 slab, more details can be found in ref. [30]. Also, the real part of the dielectric permittivity has larger values compare with the imaginary part, further increasing the screening effect [45]. Their analysis is focused on a single emission energy of the QE. On the other hand, in ref. [29], the authors report an opposite behavior where, as the number of layers of SnS_2 is increased, the SE rate also increases. This discrepancy is attributed to the fact that the MoS_2 material exhibits a band inversion from indirect, as a bulk material, to direct as a monolayer, while SnS_2 is an indirect band gap material down to a monolayer. Furthermore, in refs. [26, 29, 30], the emission profile of the QEs investigated is different for each case.

Our analysis follows a different path. Instead of using a slab for approximating the MoS_2 layer, and describing its optical response through an anisotropic dielectric permittivity, we treat the MoS_2 as a 2D material, whose optical response is given by Eq. (7). We describe the interaction between a QE and a MoS_2 superlattice using Eqs. (A2)-(A3). Multiple scattering between the MoS_2 layers of the MoS_2 creates a number of modes, depending on the number of layers. We analyze and investigate the influence these mode have on the total SE rate of the QE. We choose to investigate free standing MoS_2 superlattices for simplicity. The inclusion of the substrate will slow down the SE rate due to the difference between the substrate and superlattice dielectric permittivities. The main relaxation path for a QE is associated with the exciton polariton modes, provided by the MoS_2 superlattice. Their existence is unaffected by the inclusion of a substrate.

In Fig. 7a we present the SE rate as a function of emission energy considering the interaction between a QE and a monolayer and, double, triple and quaduple MoS_2 layers. Again we consider the case where the transition dipole moment of the QE is oriented along z. The position of the QE is fixed at $\mathbf{r}_{\text{QE}} = (0, 0, 10\,\text{nm} + D)$, where D is the distance between the top and bottom layers. We consider a fixed value of this thickness, $D = 2\,\text{nm}$, and the distance between the layers is kept equal. So as the number of layers is increased the distance between them is decreased. In Fig. 7a we observe that, as the number of layers increases, the peak value of the normalized SE rate blue-shifts and the absolute value of its enhancement decreases. The shift is smaller when the lower TM exciton polariton mode is excited. In order to give an explanation for this effect we present in Figs. (7b,7c) the dispersion relation for two superlattice examples.

As we have already discussed, the TE and TM exciton polariton modes are obtained as poles of the generalized Fresnel reflection coefficients. For a superlattice nanostructure more details are given in App. A. In Figs. (7b,7c) we present a contour plot of the logarithm of the absolute value of the reflection coefficients $R_N(k_s, \omega)$, for $E_A < \hbar\omega < 2.0\,\text{eV}$ and $\hbar\omega > E_B$, and $R_M(k_s, \omega)$, for $\hbar\omega < E_A$ and $2.0\,\text{eV} < \hbar\omega < E_B$, as a function of the in-plane wave vector, k_s, and the energy, $\hbar\omega$. The generalized reflection coefficients, R, are calculated by solving Eq. (A4). The TM mode has the largest contribution to the SE rate, see Fig. 7a. The dispersion relation lines are given by the dark color lines in the contour plot. We observe that as the number of layers increases, more branches emerge in the energy range where TM modes are supported by the MoS_2 superlattice, and the number of branches is equal the number of layers. These extra branches are connected with the multiple scatterings in the MoS_2 superlattice. In the same figure we present with a red dashed line the dispersion relation of a single MoS_2 layer for direct comparison.

The peak in the SE rate enhancement of a QE for a single layer is at $\hbar\omega = 1.95\,\text{eV}$, Fig. 7a. The main channel of relaxation of the QE, in the presence of the MoS_2 superlattice, is the TM exciton polariton mode. We choose to focus on the lower branch of the TM exciton polariton modes, related to the first peak of the normalized SE rate in Fig. 7a. The peak value for the single layer is connected with the penetration depth, $\delta_{\text{EP}}^{\text{TM}} = 1/\text{Im}\left(k_z^{\text{TM}}\right)$, where $k_z^{\text{TM}} = \sqrt{k_0^2 - k_{\text{EP}}^{\text{TM}}} \approx i k_{\text{EP}}^{\text{TM}}$ and since $k_{\text{EP}}^{\text{TM}} \gg k_0$, we find $\delta_{\text{EP}}^{\text{TM}} = 1/\text{Re}\left(k_{\text{EP}}^{\text{TM}}\right)$. In Eq. (13), the exciton polariton contribution to the SE rate depends on a factor c^2/ω^2, thus for the same value of $k_{\text{EP}}^{\text{TM}}$, there is a decrease in the absolute value of the normalized SE rate with increasing energy, explaining the trend we observe in Fig. 7a. In Figs. 7b and 7c, we show the position of the peak value of the SE rate of the QE interacting with a single MoS_2 layer and the blue arrow indicates the blue shift of the energy at which the peak value of the SE rate emerges in Fig. 7a when the double layer is considered. For the single layer, the peak of the SE rate is at $\hbar\omega = 1.95\,\text{eV}$ at $k_{\text{EP}}^{\text{TM}} = 0.1\,\text{nm}^{-1}$, $\delta_{\text{EP}}^{\text{TM}} = 10\,\text{nm}$, while for the double layer the peak is at $\hbar\omega = 1.97\,\text{nm}$ and for the triple layer it is at $\hbar\omega = 1.98\,\text{nm}$. Thus the dispersion relations give an explanation for the blue shift of the peak value of the normalized SE rate.

Therefore, to investigate the interaction between a specific QE and a MoS_2 supelattice, one must take into account the reduced interaction between QEs–MoS_2 superlattice as one starts increasing the number of layers. While the emission

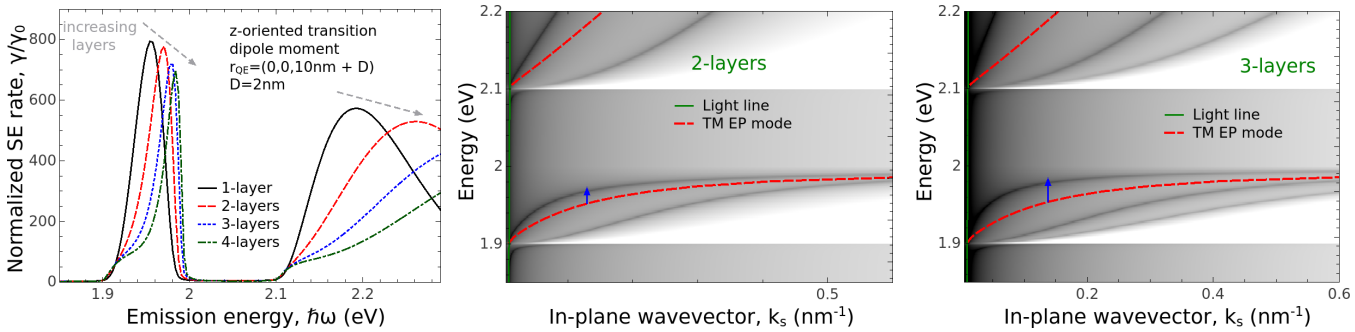

(a) (b) (c)

Figure 7: (Color online) (a) Total normalized spontaneous emission of a QE, placed at a fixed position, $\mathbf{r}_{\rm QE} = (0,0,10\,{\rm nm}+D)$, as a function of its emission energy, considering different numbers of MoS_2 layers. The transition dipole moment of the QE is z-oriented. (b-c) Dispersion relation, $k_s(\omega)$, showing $\log(|R_N|)$, for ${\rm Im}(\sigma_{\rm res}) > 0$, and $\log(|R_M|)$, for ${\rm Im}(\sigma_{\rm res}) < 0$, considering multiple MoS_2 layers. (b) 2-layers. (d) 3-layers. D is the thickness between the lower and upper MoS_2 layers, here $D = 2\,{\rm nm}$. The dispersion relation of the TM exciton polariton mode of a single MoS_2 layer is presented with a red dashed line line. The damping parameters have the values, $\gamma_B = 0.3\,{\rm meV}$ and $\gamma_A = 0.7\,{\rm meV}$.

properties of the QE do not change, its environment is modified as there is a redistribution of the available modes. The dispersion relation plays a crucial role in explaining this effect, giving us the available modes that can be supported.

To further analyze this effect, in Fig. 8 we present contour plots of the logarithm of the absolute value of the electric field, $E_z(\mathbf{r},\omega) \propto \mathfrak{G}_{zz}(\mathbf{r},\mathbf{r}_{\rm QE},\omega)$, created by a QE placed at $\mathbf{r}_{\rm QE} = (0,0,10\,{\rm nm}+D)$, in the presence of a MoS_2 superlattice, $D = 2\,{\rm nm}$ in our case. The emission energy of the QE has been selected to be at the maximum value of the SE rate for a single MoS_2 layer, $\hbar\omega = 1.95\,{\rm eV}$. The scale of the color maps in Fig. 8 is the same in all panels, for direct comparison. We observe that the field intensity decreases as the number of the MoS_2 layers increases. This is due to the poorer coupling of the near field of the QE to the MoS_2 superlatice. We observe also that the extent of the field in the x direction decreases as the number of layers is increased. The propagation length for the single layer is $L_{\rm EP}^{\rm TM} = 373\,{\rm nm}$ while for the double layer it is $L_{\rm EP}^{\rm TM} = 300\,{\rm nm}$, and, as the number of layers further increases, the propagation length further reduces.

The opposite behavior can be observed when the QE emission energy is at the maximum value of the SE rate for a MoS_2 superlattice, e.g. for the three-layer superlattice. Then the SE rate of the QE decreases with decreasing the number of layers. For this example of the trilayer, at the resonance $\hbar\omega = 1.98$, the normalized SE rate is $\tilde{\Gamma} = 718$, compared with $\tilde{\Gamma} = 444$ for the two layer and $\tilde{\Gamma} = 102$ for a monolayer.

IV. CONCLUSIONS AND FUTURE WORK

In this contribution we have investigated the spectral and distance dependence of the SE rate of a QE in the presence of a MoS_2 layer and superlattice. A MoS_2 layer supports transverse electric and transverse magnetic surface exciton polariton modes. The TM modes are strongly confined to the MoS_2 layer and have long propagation lengths. The TE modes are only loosely confined to the MoS_2 layer.

The total SE rate of the QE in the presence of a MoS_2 layer is analyzed with respect to the different contributions, namely, the lossy surface wave, surface exciton polariton and radiative emission. In the main part of the discussion we showed that the existence of TE and TM exciton polariton modes is connected with the surface conductivity of the MoS_2, specifically with the sign of its imaginary part. For energies at which the TM exciton polariton modes are excited, the SE rate of a QE is enhanced several order of magnitude, compared with its free-space value. For all the emission energies of the QE, the main contribution to the SE comes from the LSW at small separations, but their contribution dies out fast as the separation is increased. When the TM modes are excited, they dominate at intermediate distances, 6 nm to 100 nm. For distances at which the LSW are not excited or above the penetration depth of the TM exciton polariton modes, the QE radiates to the far field.

Next, the interaction between a QE and a MoS_2 superlattice is investigated. We observe a blue-shift of the peak value of the SE rate of the QE, as a function of its emission energy, as we increase the number of MoS_2 layers from one to four. Using the dispersion relation plot, this blue-shift is explained. It is seen that the number of layers determines the number of branches of the exciton polariton modes available. The blue-shift of the SE rate is connected with the blue-shift of the dispersion line for the MoS_2 superlattice, compared with the single layer. For a QE with emission energy corresponding to the peak energy of the SE rate for the monolayer, as the number of layers is increased the coupling decreases and the field intensity distribution around the superlattice decreases. The opposite behavior is observed if the emission energy of the QE is on resonance with a MoS_2 superlattice.

Although the results presented in this study focused on MoS_2 as a material, they are quite general and can be applied to any material whose optical properties are determined by exciton generation. Thus, they can be applied to any of the rest of the TMD family. Furthermore, we have choosen to con-

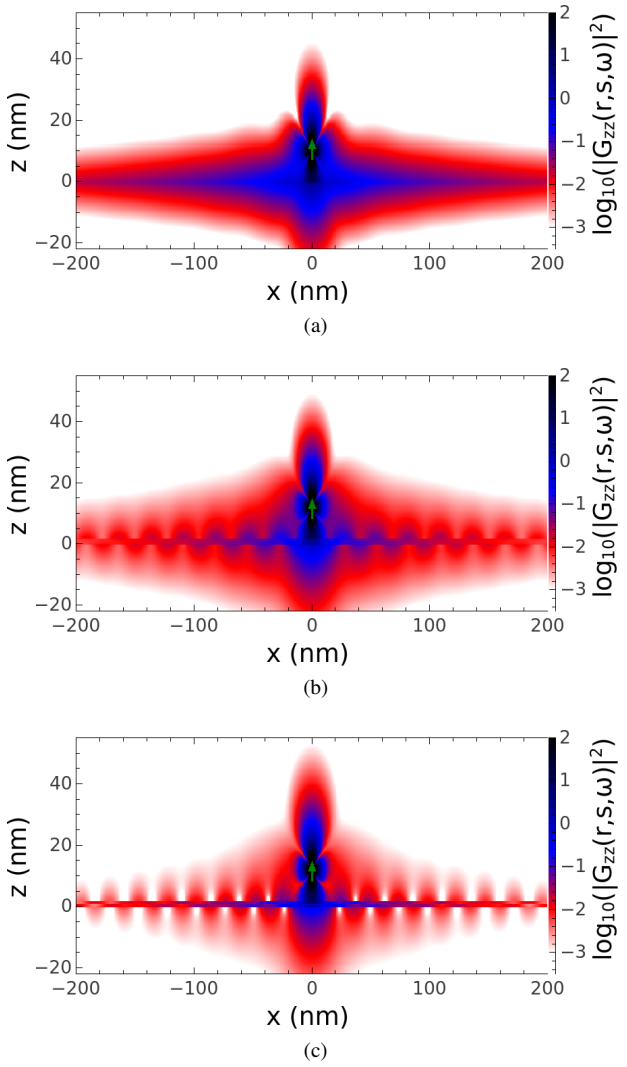

Figure 8: (Color online) Contour plots of the logarithm of the field intensity, $\log_{10}\left(|G_{zz}(\mathbf{r},\mathbf{s},\omega)|^2\right)$, created by a QE, placed at $\mathbf{s}=(0,0,D+10\,\text{nm})$. The transition dipole moment of the QE is along z and its emission energy is $\hbar\omega=1.915\,\text{eV}$. (a) Single layer, (b) Double layer, (c) Triple layer. The damping parameters have the values, $\gamma_B=0.3\,\text{meV}$ and $\gamma_A=0.7\,\text{meV}$.

centrate on a theoretical investigation of the MoS_2, and not to fit existing experimental data. This is due to the fact that the material parameters are strongly influenced by the quality of the material sample itself.

This study made a contribution to explaining all the contradictory results regarding the spectral and distance dependences of QEs in the presence of MoS_2 layers. Specifically, we presented a z^n, $n=2,3,4$, distance dependence of the SE rate of a QE, which is connected with the LSWs at the different emission energies. Also we observed the existence of exciton polariton modes and how they modify the emission properties of QEs and the strength of the interaction, where the distance dependence follows the expression $\sim\exp\left(-2z/\delta_{EP}^{TM}\right)$. Moreover, we explained that the coupling of a QE with a MoS_2 superlatice depends on its emission energy. The peak value for the SE rate of a QE blue-shifts depending on the number of MoS_2 layers, due to the different mode distribution supported by these structures. While the emission properties of the QE remain the same, the modes provided by the environment change as the number of MoS_2 layers changes. Depending on the emission energy of the QE, the SE rate can increase or decrease as the number of MoS_2 layers is increased. Dielectric screening can explain certain results for certain emission energies of the QE.

Multilayer devices based on MoS_2 and graphene can be the precursors of an all-optical device. Graphene's optical properties can be tuned by changing its chemical potential, but it has small absorption in the visible part of the optical spectrum. Combining graphene with TMD layers allows one access to the best of both materials for applications like light harvesting and light emitting devices [46, 47]. In general the total absorption of these two materials can be further enhanced by including also layers of QEs. The emission properties of the QEs can be chosen depending on the nature of the application. For light harvesting devices we need the emission energy of the QEs to maximize the non-radiative energy transfer to the MoS_2 layer, where the generated electron-hole pair will be harvested. On the other hand, for LEDs we need to maximize the far field emission of the SE rate of the QEs. Both of these effects can be further investigated for devices composed from patterned 2D nanostructures, like ribbons and disks, where the redistribution of the available modes gives rise to sharp resonances [48, 49].

Acknowledgments

This work was supported by the Science Foundation Ireland under grant No. 10/IN.1/12975.

Appendix A: Green's tensor for a MoS_2 superlattice

A multilayer planar geometry is considered, which consists of a number of N layers, indexed by their layer number $i=1,\ldots,N$ where each layer has thickness d_i and dielectric permittivity ε_i. The layers are of infinite extent in the xy plane and the z axis is perpendicular to the surface of each layer.

The method of scattering superposition is used [50, 51] where the Green's tensor splits into two parts:

$$\mathfrak{G}(\mathbf{r},\mathbf{s},\omega)=\mathfrak{G}_h(\mathbf{r},\mathbf{s},\omega)+\mathfrak{G}_s(\mathbf{r},\mathbf{s},\omega), \tag{A1}$$

where $\mathfrak{G}_h(\mathbf{r},\mathbf{s},\omega)$ is the homogeneous part that accounts for direct interaction between the source and target point at $\mathbf{s}$ and $\mathbf{r}$ respectively, and is non-zero when both points are in the same media and there is no discontinuity between them. $\mathfrak{G}_s(\mathbf{r},\mathbf{s},\omega)$ is the scattering part, is always present and accounts for the multiple reflections and transmissions taking place at the interfaces.

The general form of the scattering part of the Green's tensor has the form:

$$\mathfrak{G}_s(\mathbf{r},\mathbf{s},\omega) = \frac{i}{8\pi^2}\int \mathrm{d}^2k_s \frac{1}{k_{zi}k_s^2}\sum_T R_T^{\pm(ij)\pm}\mathbf{T}(\mathbf{k}_s,\pm k_{zi},\mathbf{r})\otimes\mathbf{T}^*(\mathbf{k}_s,\pm k_{zj},\mathbf{s}). \tag{A2}$$

A summation is implied for each pair of $\pm$ indices. These indices show the direction of propagation of the electromagnetic modes, the first index for the acceptor and the second for the donor. Also the summation over $\mathbf{T}$ is over the $\mathbf{M}$ and $\mathbf{N}$ modes which are connected with the transverse electric and transverse magnetic modes, respectively. The form of $\mathbf{M}$ and $\mathbf{N}$ can be found in ref. [51]. For the planar geometries there are no hybrid modes. The boundary conditions imposed on the system of multilayers are the continuity condition and the radiation condition. The first condition is given by continuity equations at each interface:

$$\hat{\mathbf{z}}\times\left[\mathfrak{G}^{(ij)}(\mathbf{r},\mathbf{s},\omega)-\mathfrak{G}^{((i+1)j)}(\mathbf{r},\mathbf{s},\omega)\right]\Big|_{z=d_i}=0, \tag{A3a}$$

$$\hat{\mathbf{z}}\times\left[\nabla\times\mathfrak{G}^{(ij)}(\mathbf{r},\mathbf{s},\omega)-\nabla\times\mathfrak{G}^{((i+1)j)}(\mathbf{r},\mathbf{s},\omega)\right]\Big|_{z=d_i}=-i\frac{4\pi}{c}k_0\sigma\hat{z}\times\hat{z}\times\mathfrak{G}^{((i+1)j)}(\mathbf{r},\mathbf{s},\omega), \tag{A3b}$$

where σ is the surface conductivity of the 2 dimensional material, for our case it is the MoS_2 layer, Eq. (7).

By applying these boundary equations, an inhomogeneous system of 2^{N-1} equations is defined which have 2^{N-1} unknowns, the generalized $R_{M(N)}^{\pm(ij)\pm}$ coefficients. These coefficients are sufficient to uniquely determined the problem under consideration through the exact knowledge of the scattering part of the Green's tensor. In order to find the generalized coefficients, a matrix equation is solved which has the form

$$\Delta_{M(N)}\cdot R_{M(N)}^{(i)\pm}=V_{M(N)}^{(i)\pm}, \tag{A4}$$

where Δ is the characteristic matrix of the system of equations from the boundary conditions at the interfaces, $R^{(i)\pm}$ is the column of the generalized coefficients $R_{M(N)}^{\pm(ij)\pm}$ and $V^{(i)\pm}$ is the free term vector whose terms are given by the homogeneous part of the Green's tensor.

We will consider in more detail the case where a 2D material, MoS_2, is sandwiched between two planar half-spaces with dielectric permittivities ε_1 and ε_2. The z-direction is perpendicular to the boundary between the two half-spaces[51, 52]. Using Eq. (A1) the Green's tensor has the form

$$\mathfrak{G}^{(11)}(\mathbf{r},\mathbf{s},\omega)=\mathfrak{G}_h^{(11)}(\mathbf{r},\mathbf{s},\omega)+\mathfrak{G}_s^{(11)}(\mathbf{r},\mathbf{s},\omega), \tag{A5a}$$

$$\mathfrak{G}^{(21)}(\mathbf{r},\mathbf{s},\omega)=\mathfrak{G}_s^{(21)}(\mathbf{r},\mathbf{s},\omega), \tag{A5b}$$

where the first of the two labels in the superscript $(i1)$ denotes the field point, while the second denotes the source point. The scattering terms have the following expression

$$\mathfrak{G}_s^{(11)}(\mathbf{r},\mathbf{s},\omega)=\frac{i}{8\pi^2}\sum_K\int \mathrm{d}^2k_s\frac{1}{k_{z1}k_s^2}R_K^{+11-}\mathbf{K}(k_s,k_{z1},\mathbf{r})\otimes\mathbf{K}^*(k_s,-k_{z1},\mathbf{s}) \tag{A6a}$$

$$\mathfrak{G}_s^{(21)}(\mathbf{r},\mathbf{s},\omega)=\frac{i}{8\pi^2}\sum_K\int \mathrm{d}^2k_s\frac{1}{k_{z1}k_s^2}R_K^{-21-}\mathbf{K}(k_s,-k_{z2},\mathbf{r})\otimes\mathbf{K}^*(k_s,-k_{z1},\mathbf{s}) \tag{A6b}$$

where $k_s=\sqrt{k_i^2-k_{zi}^2}$ is the in-plane propagation constant, k_{zi} is the perpendicular propagation constant in medium i, and $k_i=\frac{\omega}{c}\sqrt{\varepsilon_i}$ is the wavenumber in medium i $(i=1,2)$. The above expressions involve a summation over $\mathbf{K}$ which represents $\mathbf{M}$ and $\mathbf{N}$, the transverse electric (TE) and transverse magnetic (TM) modes, respectively.

Imposing the continuity conditions, Eq. (A5), at the boundary between the two half spaces, $z=0$, we obtain the generalized Fresnel coefficients, which have the form [35, 36],

$$R_M^{11}=\frac{k_{z1}-k_{z2}-2\alpha k_0}{k_{z1}+k_{z2}+2\alpha k_0},\quad R_N^{11}=\frac{k_2^2k_{z1}-k_1^2k_{z2}+2\alpha k_0k_{z1}k_{z2}}{k_2^2k_{z1}+k_1^2k_{z2}+2\alpha k_0k_{z1}k_{z2}} \tag{A7a}$$

$$R_M^{21}=\frac{2k_{z1}}{k_{z1}+k_{z2}+2\alpha k_0},\quad R_N^{21}=\frac{2k_1k_2k_{z1}}{k_2^2k_{z1}+k_1^2k_{z2}+2\alpha k_0k_{z1}k_{z2}}, \tag{A7b}$$

where $\alpha = 2\pi\sigma/c$.

[1] E. Purcell, Phys. Rev. **69**, 681 (1946).
[2] S.A. Maier, and H.A. Atwater, J. Appl. Phys. **98**, 011101 (2005).
[3] C.A. Marocico and J. Knoester, Phys. Rev. A **84**, 053824 (2011).
[4] J.B. Khurgin, Nat. Nanotechnol. **10**, 2 (2015).
[5] T. Low and P. Avouris, ACS Nano **8**, 1086 (2014).
[6] F.J. García de Abajo, ACS Photonics **1**, 135 (2014).
[7] P. Avouris, Nano Lett. **10**, 4285 (2010).
[8] L. Gaudreau, K.J. Tielrooij, G.E.D.K. Prawiroatmodjo, J. Osmond, F.J.G. de Abajo, and F.H.L. Koppens, Nano Lett. **13**, 2030 (2013).
[9] J. Lee, W. Bao, L. Ju, P.J. Schuck, F. Wang, and A. Weber-Bargioni, Nano Lett. **14**, 7115 (2014).
[10] F. Yang, J.R. Sambles, and G.W. Bradberry, Phys. Rev. Lett. **64**, 559 (1990).
[11] J.D. Caldwell, L. Lindsay, V. Giannini, I. Vurgaftman, T.L. Reinecke, S.A. Maier, and O.J. Glembocki, Nanophotonics **4**, 1 (2015).
[12] A. Scholz, T. Stauber, and J. Schliemann, Phys. Rev. B **88**, 035135 (2013).
[13] Y.N. Gartstein, X. Li, and C. Zhang, Phys. Rev. B **92**, 075445 (2015).
[14] J. B. Khurgin, Optica **2**, 740 (2015).
[15] L. Britnell, R.M. Ribeiro, A. Eckmann, R. Jalil, B.D. Belle, A. Mishchenko, Y.-J. Kim, R.V. Gorbachev, T. Georgiou, S.V. Morozov, A.N. Grigorenko, A.K. Geim, C. Casiraghi, A.H.C. Neto, and K.S. Novoselov, Science **340**, 1311 (2013).
[16] F. Xia, H. Wang, D. Xiao, M. Dubey, and A. Ramasubramaniam, Nat. Photon. **8**, 899 (2014).
[17] D. Xiao, G.B. Liu, W. Feng, X. Xu, and W. Yao, Phys. Rev. Lett. **108**, 196802 (2012).
[18] H. Yu, G.-B. Liu, P. Gong, X. Xu, and W. Yao, Nat. Commun. **5**, 1 (2014).
[19] O. Lopez-Sanchez, D. Lembke, M. Kayci, A. Radenovic, and A. Kis, Nat. Nanotechnol. **8**, 497 (2013).
[20] D. Kozawa, R. Kumar, A. Carvalho, K. Kumar Amara, W. Zhao, S. Wang, M. Toh, R.M. Ribeiro, A.H. Castro Neto, K. Matsuda, and G. Eda, Nat. Commun. **5**, 4543 (2014).
[21] C. Chakraborty, L. Kinnischtzke, K.M. Goodfellow, R. Beams, and A.N. Vamivakas, Nat. Nanotechnol. **10**, 507 (2015).
[22] M. Amani, D.-H. Lien, D. Kiriya, J. Xiao, A. Azcatl, J. Noh, S.R. Madhvapathy, R. Addou, S. KC, M. Dubey, K. Cho, R.M. Wallace, S.-C. Lee, J.-H. He, J.W. Ager, X. Zhang, E. Yablonovitch, and A. Javey, Science **350**, 1065 (2015).
[23] K. Messer, M. Eggleston, S.B. Desai, S.A. Fortuna, S. Madhavapathy, P. Zhao, J. Xiao, X. Zhang, A. Javey, M.C. Wu, and E. Yablonovitch, 2015 Fourth Berkeley Symposium on Energy Efficient Electronic Systems (E3S) IEEE, 1 (2015).
[24] M.I. Vasilevskiy, D.G. Santiago-Pérez, C. Trallero-Giner, N.M.R. Peres, and A. Kavokin, Phys. Rev. B **92**, 245435 (2015).
[25] B. Radisavljevic, A. Radenovic, J. Brivio, V. Giacometti, and A. Kis, Nat. Nanotechnol. **6**, 147 (2011).
[26] F. Prins, A.J. Goodman, and W.A. Tisdale, Nano Lett. **14**, 6087 (2014).
[27] D. Kufer, I. Nikitskiy, T. Lasanta, G. Navickaite, F.H.L. Koppens, and G. Konstantatos, Adv.Mater. **27**, 176 (2015).
[28] S. Sampat, T. Guo, K. Zhang, J.A. Robinson, Y. Ghosh, K.P. Acharya, H. Htoon, J.A. Hollingsworth, Y.N. Gartstein, and A.V. Malko, ACS Photonics **3**, 708 (2016).
[29] H. Zang, P.K. Routh, Y. Huang, J.-S. Chen, E. Sutter, P. Sutter, and M. Cotlet, ACS Nano **10**, 4790 (2016).
[30] A. Raja, A. Montoya-Castillo, J. Zultak, X.-X. Zhang, Z. Ye, C. Roquelet, D.A. Chenet, A.M. van der Zande, P. Huang, S. Jockusch, J. Hone, D.R. Reichman, L.E. Brus, and T.F. Heinz, Nano Lett. **16**, 2328 (2016).
[31] K.M. Goodfellow, C. Chakraborty, K. Sowers, P. Waduge, M. Wanunu, T. Krauss, K. Driscoll, and A. N. Vamivakas, Appl. Phys. Lett. **108**, 021101 (2016).
[32] C. Zhang, H. Wang, W. Chan, C. Manolatou, and F. Rana, Phys. Rev. B **89**, 205436 (2014).
[33] H.T. Dung, L. Knöll, and D.-G. Welsch, Phys. Rev. A **57**, 3931 (1998).
[34] H.T. Dung, L. Knöll, and D.-G. Welsch, Phys. Rev. A **62**, 053804 (2000).
[35] G.W. Hanson, J. Appl. Phys. 103, 064302 (2008).
[36] A.Y. Nikitin, F.J. Garcia-Vidal, and L. Martin-Moreno, IEEE J. Select. Topics Quantum Electron. **19**, 4600611 (2013).
[37] M. Palummo, M. Bernardi, and J.C. Grossman, Nano Lett. **15**, 2794 (2015).
[38] T. Stauber, D. Noriega-Pérez, and J. Schliemann, Phys. Rev. B **91**, 115407 (2015).
[39] S.A. Mikhailov and K. Ziegler, Phys. Rev. Lett. **99**, 016803 (2007).
[40] G.W. Hanson, S.A. Hassani Gangaraj, C. Lee, D.G. Angelakis, and M. Tame, Phys. Rev. A **92**, 013828 (2015).
[41] V.D. Karanikolas, C.A. Marocico, and A.L. Bradley, Phys. Rev. B **91**, 125422 (2015).
[42] J.A. Dionne, L.A. Sweatlock, H.A. Atwater, and A. Polman, Phys. Rev. B **72**, 075405 (2005).
[43] V. Agranovich, H. Benisty, and C. Weisbuch, Solid State Commun. **102**, 631 (1997).
[44] G.W. Ford and W.H. Weber, Phys. Rep. **113**, 195 (1984).
[45] J.M. Gordon and Y.N. Gartstein, J. Phys. Condens. Matter **25**, 425302 (2013).
[46] H. Wang, H. Feng, and J. Li, Small **10**, 2165 (2014).
[47] S.-G. Yi, J. H. Kim, J.K. Min, M. J. Park, Y. W. Chang, and K.-H. Yoo, IEEE Trans. Nanotech. **15**, 499 (2016).
[48] T. Christensen, W. Yan, A.-P. Jauho, M. Wubs, and N.A. Mortensen, Phys. Rev. B **92**, 121407 (2015).
[49] V.D. Karanikolas, C.A. Marocico, and A.L. Bradley, Phys. Rev. B **93**, 035426 (2016).
[50] C. T. Tai, *Dyadic Green Functions in Electromagnetic Theory* (IEEE Press, New York, NY, USA, 1994).
[51] W. C. Chew, *Waves and Fields in Inhomogeneous Media* (IEEE Press, New York, NY, USA, 1995).
[52] L. Novotny and B. Hecht, *Principles of nano-optics*, 2nd ed. (Cambridge University Press, Cambridge, UK, 2012).